Journal of Materials Science: Materials in Electronics
https://doi.org/10.1007/s10854-020-03886-7

A study on $CdCl_2$ activation of CBD-CdS films

W. G. C. Kumarage[1] · R. P. Wijesundera[2] · V. A. Seneviratne[3,4] · C. P. Jayalath[3,4] · N. Kaur[5] · E. Comini[5] · N. Gunawardhana[1] · B. S. Dassanayake[3,4]

Received: 12 April 2020 / Accepted: 26 June 2020

Abstract
Cadmium sulfide (CdS) thin films were deposited using chemical bath deposition (CBD) technique on fluorine-doped tin oxide glass substrates. Cadmium sulfate, thiourea, and ammonium hydroxide were used as Cd source, S source, and the complexing agent, respectively in the reaction bath. The post-deposition $CdCl_2$ activation of chemical bath deposited CdS (CBD-CdS) thin films was done by dip coating in a saturated $CdCl_2$ bath. X-ray diffractograms show the growth of large CdS grains with better crystalline quality over the recrystallization process due to $CdCl_2$ treatment. The development of large clusters was determined to be due to coalescence of smaller clusters. The photoelectrochemical (PEC) cell ($CdS/Na_2S_2O_3$/Pt) parameters, such as V_{OC} and I_{SC} for $CdCl_2$ activated CBD-CdS thin films were found to be higher compared to untreated CBD-CdS thin films. The improved effective surface area of the film and higher carrier concentration due to grain boundary passivation could be the reason for higher V_{OC} and I_{SC} values found in $CdCl_2$-treated CdS films. Additionally, all the $CdCl_2$-treated CdS films showed an increase in the optical transmittance spectra and bandgap compared to untreated CdS films. Relative energy band edge position of the grown CdS films was found to be adjustable with the $CdCl_2$ treatment time. The best photoactivity was found for the CdS films which were dip-coated for 10 min in $CdCl_2$ solution.

1 Introduction

Polycrystalline CdS thin films have shown potential photovoltaic applications due to its direct bandgap, high transmittance, low resistivity, and relative ease of film growth [1, 2]. Among the dozens of growth techniques, chemical bath deposition (CBD) is considered as a favored technique of CdS thin film deposition due to its simplicity, low cost, adaptability, and reliability [3–8]. Additionally, the effect on growth kinetics, deposition bath temperature, chemical concentration, film thickness, and surface morphology to achieve improved photo active CBD-CdS thin film has been comprehensively reported in previous studies [9–12]. Subject to the growth condition and technique, CdS film can be found in either metastable cubic or highly stable hexagonal phase [13]. Since better crystallinity of the window layer in photovoltaic devices is a must to achieve superior light to current efficiency, it is crucial to improve the crystallinity of CdS to produce superior devices [2, 14].

$CdCl_2$ heat treatment on CdTe is well known since the 1970s to improve the conversion efficiency of CdTe/CdS solar cells [15–17]. Also, $CdCl_2$ treatment offers several significant benefits such as grain boundary passivation, increase of grain size, reduction of lattice mismatch between the CdS and CdTe layers, resulting in improved efficiency of conversion of light to current in the CdS/CdTe solar cells [18]. However, few articles have been reported the $CdCl_2$ heat treatment on CdS [19]. Among different types of post deposition heat treatment methods, $CdCl_2$ treatment on CdS thin films can be considered as a crucial method to grow high-quality CdS thin films [19].

Conventionally, there are three major $CdCl_2$ treatment methods; wet treatment [20], evaporated treatment [21], and vapor treatment [22]. In this manuscript, a comprehensive investigation is reported on conventional wet treatment on

✉ B. S. Dassanayake
buddhikad@pdn.ac.lk

1 Research and International Affairs, Sri Lanka Technological Campus, Padukka, Sri Lanka

2 Department of Physics, University of Kelaniya, Kelaniya, Sri Lanka

3 Postgraduate Institute of Science, University of Peradeniya, Peradeniya, Sri Lanka

4 Department of Physics, University of Peradeniya, Peradeniya, Sri Lanka

5 Department of Information Engineering, Università Degli Studi Di Brescia, Brescia, Italy

Published online: 14 July 2020

chemical bath deposited CdS (CBD-CdS) by the means of photoelectochemical (PEC) cell measurements, *C–V* measurements, field emission scanning electron microscopy (FE-SEM), optical measurements, and grazing incidence X-ray diffraction (GIXRD).

2 Experiment

0.001 mol dm^{-3} $3CdSO_4{\cdot}8H_2O$ (cadmium sulfate, Sigma Aldrich, 99%, USA), 0.002 mol dm^{-3} $CS(NH_2)_2$ (thiourea, Sigma Aldrich, 99%, USA) and 1.1 ml NH_3 (ammonia, Sigma Aldrich, 35% w/w, USA) were used as the starting chemical for the growth of CBD-CdS thin films. Bath temperature was kept at 80 °C for 1 h over the course of CBD process using FTO (~ 10 Ω /□, TEC 10, Sigma Aldrich, USA) glass substrates. Cleaning of the substrate and grown films was carried out according to the procedure explained in Kumarage et al.[23]. All the grown CdS thin films were about 80 nm in thickness. Later, the grown films underwent dip coating with saturated $CdCl_2$-methanol ($CdCl_2$, Fluka, 99%, USA; methanol, Sigma Aldrich, 99.8%, USA) solution. The $CdCl_2$ treatment duration was varied from 2 to 20 min. Later, all the grown films were annealed at 200 °C for 1 h. The coding of the grown films corresponding to the treatment duration time is denoted in Table 1.

3 Characterizations

The morphological study of the grown CdS films was done using an FE-SEM model LEO 1525. All the GIXRD analysis of grown films were examined in a PANalytical diffractometer (Empyrean) with a monochromatic beam of CuKα ($\lambda = 1.54184$ Å) with 2° incident angle, working under 40 mA tube current at 40 kV. UV-1800 Shimadzu spectrophotometer was employed to examine the optical properties of the grown CdS films in the optical window of 300–800 nm. Profilometer (XP-1) was used to measure the thickness of grown CdS films. All the photoelectrochemical (PEC) cell analyses were carried out for the structure of Pt/$Na_2S_2O_3$/CdS/ FTO using PEC Cell L01. A 150 W short-arc xenon lamp was used to illuminate the CdS/electrolyte junction. The same PEC cell configuration was used for the *C–V* measurements. A sinusoidal signal of 1000 Hz with a voltage of 20 mV corresponding to the Ag/AgCl electrode was used to bias the CdS/electrolyte junction. The electrolyte used for all the electrical characterizations was 0.1 mol dm^{-3} $Na_2S_2O_3$ (Baxter Smith Labs, 97%, USA) and the semiconductor to electrolyte contact area was 0.25 cm^2.

Table 1 CdS film codes and the dipping durations for $CdCl_2$ treatment

Dipping duration (minutes)	CdS film code
0	S-0
2	S-2
6	S-6
10	S-10
14	S-14
18	S-18
20	S-20

4 Results and discussion

4.1 Optical measurements

The optical bandgap (E_g) values of the grown films were calculated by extrapolating the straight portions of the curves of $(\alpha h\nu)^2$ vs. $h\nu$ onto the "hν" axes using the Stern relation [24–27]:

$$\alpha = A\frac{\left(h\nu - E_g\right)^{n/2}}{h\nu} \quad (1)$$

where α is the optical absorption coefficient, h is the Plank's constant, A is a constant and for direct bandgap materials such as CdS, n is equal to 1. Variation of E_g of the grown CdS thin films corresponding to the $CdCl_2$ dipping times is shown in Fig. 1. The film S-10 demonstrations the highest value of 2.41 eV in E_g, whereas the lowest 2.33 eV was observed in S-0. The variation in E_g of CBD-CdS thin films could be associated with changes in the lattice strain due to the recrystallization as a result of $CdCl_2$ heat treatment [28]. Additionally, the results propose that the E_g values of

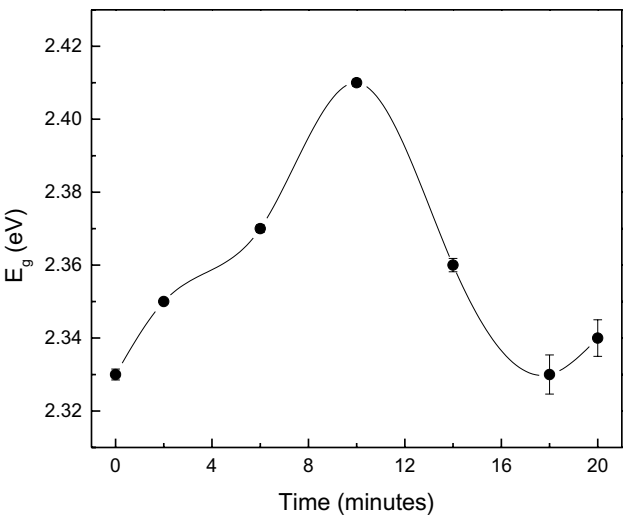

Fig. 1 E_g variation of the $CdCl_2$-treated CdS thin films

the CBD-CdS can be tuned between 2.33 and 2.41 eV by varying the $CdCl_2$ treatment time.

The optical transmittance results in the optical window of 300–800 nm of the grown CdS on FTO corresponding to $CdCl_2$ treatment times are presented in Fig. 2. The optical transmittance edge of all the $CdCl_2$ activated films shows a blue-shift compared to the untreated, justifying the alteration of E_g value with the $CdCl_2$ treatment time observed in Fig. 1. Further, it can also be seen that all the $CdCl_2$ activated films have comparatively high transmittance below the optical bandgap compared to the untreated films, though the films are in the same thickness range. The highest optical transmittance was yielded for the films grown with a $CdCl_2$ treatment time of 10 min. The improvements in the optical transmittance also suggests low concentration of defects and better CdS crystal quality. The improvement in the crystal quality may diminish the absorption of light in the longer wavelength region, subsequently enhance the electrical properties [27, 29].

4.2 Structural characterization

Figure 3 shows GIXRD diffractograms of (a) $CdCl_2$-treated film which showed the highest optical bandgap and the highest transmittance, (b) untreated CBD-CdS, and (c) bare FTO glass. Results suggest that the deposited CBD-CdS films are in the hexagonal phase. Five diffraction peaks were found to originate from diffraction angles 25.07˚, 26.46˚, 28.32˚, 44.10˚ and 48.34˚. The peaks were identified to be hexagonal reflections of (100), (002), (101), (110) and (103) planes of CdS (JCPDS 98–009-5006). The rest of the peaks belong to the FTO substrate. Figure 3a and Table 2 show the existence of broad asymmetric peaks (25.19˚, 26.52˚ and 44.18˚) in $CdCl_2$-treated films with a tail extending towards higher

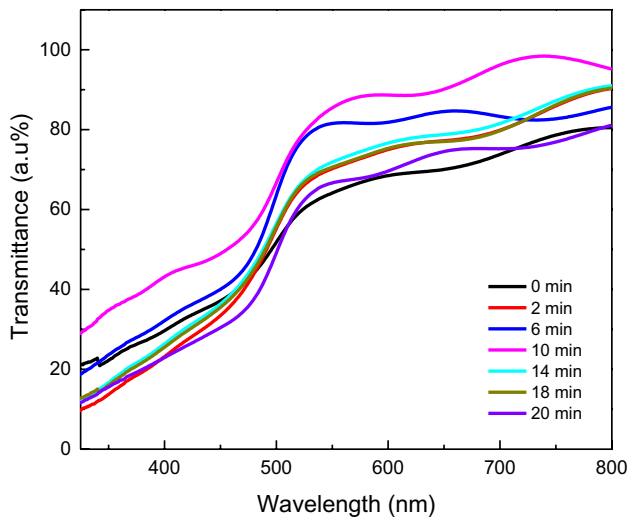

Fig. 2 Transmittance variation of the $CdCl_2$-treated CdS thin films

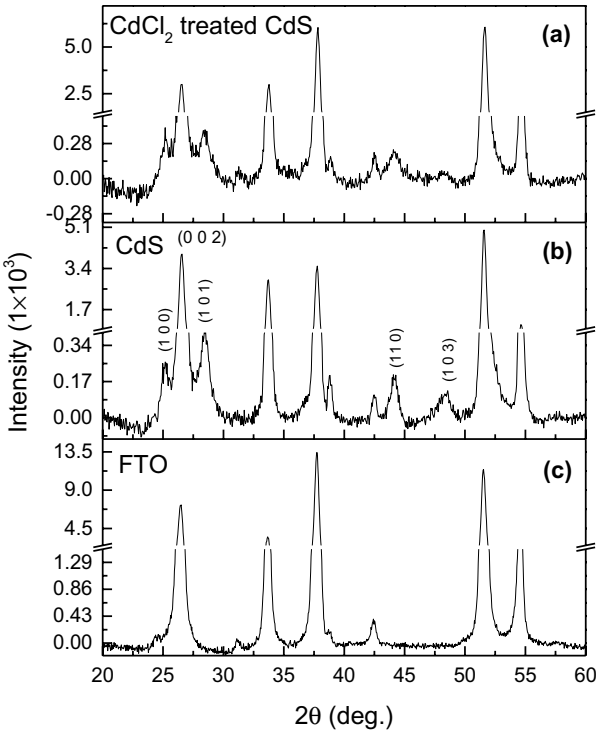

Fig. 3 GIXRD diffractograms of **a** $CdCl_2$-treated CdS, **b** CdS on FTO **c** Bare FTO glass

angles. These asymmetric peaks can be originating from the primary recrystallization of CdS due to broken Cd-S bonds since $CdCl_2$ behaves as a fluxing agent [29]. Hence it is worth to discuss the mechanism that could potentially affect the recrystallization.

Conventionally, there is an excess number of sulfur vacancies in CdS films associated with that of the interstitial cadmium (Cd_i). The chemical route of forming Cd_i and releasing S from the CdS along with the $CdCl_2$ treatment can be explained as follows [19]:

$$CdS + CdCl_2 \rightarrow 2Cl_s + 2Cd_i + 1/2S_{2(g)} \quad (2)$$

where X_i and X_s denote the interstitial position and substitutional position of an element respectively. Hence, a significant quantity of Cl atoms diffuses into the CdS films along

Table 2 Two theta angle and the corresponding reflection plane

Plane	Untreated CdS		$CdCl_2$-treated CdS (S-10)	
	2θ (°)	d (Å)	2θ (°)	d (Å)
100	25.1196	3.54522	25.1960	3.53464
002	26.4882	3.36506	26.5289	3.35999
110	44.1554	2.05111	44.1835	2.04987

with the annealing process and create Cl_s state. Furthermore, with the introduction of Cl_s state in the CdS, V_{Cd}^{2+} and Cl_s are formed to create deep and shallow levels (V_x denote a vacancy) [30]. Thereby it can be concluded here, most of the sulfur vacancies are chemically engaged by the Cl^- ions to form Cl_s. As the Cl_s occupied in V_s, it prevents oxygen incorporation on CdS during the $CdCl_2$ treatment. Thereby in the annealing process, nanoscale grains will coalesce to form a dense film [19]. Also, Cd vacancies are created in the CdS matrix to maintain the overall charge neutrality along with the incorporation of Cl^- ions. This formation of Cd vacancies enables enough space for the rearrangement of atoms during the recrystallization process, promoting coalescence of neighboring clusters.

In order to examine the preferential crystallite alignment of the grown CdS films, the texture coefficient (TC_{hkl}) of $CdCl_2$-treated (10 min) films and untreated was calculated. For the TC_{hkl} calculation following equation was used [31–35]:

$$TC_{hkl} = \frac{I_{(hkl)}/I_{0(hkl)}}{1/n\left[\sum_{i=1}^{n} I_{(hkl)}/I_{0(hkl)}\right]} \quad (3)$$

where n is the number of X-ray diffraction peaks, $I_{(hkl)}$ is the measured intensity and $I_{0(hkl)}$ is the standard intensity of the plane (hkl). The standard intensity of the plane (hkl) was taken from the JCPDS 98-009-5006. The TC_{hkl} for films S-0 and S-10 are displayed in Fig. 4. The figure illustrates that the relative intensity of the peaks (100) and (101) increase with the $CdCl_2$ treatment, while the intensity of (002) decreases. Yet, the results indicate that the reflection plane (002) seems to be the favored orientation for both investigated films S-0 and S-10.

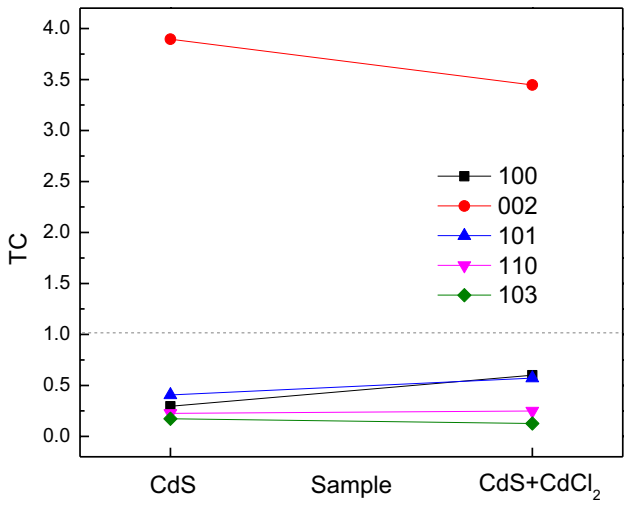

Fig. 4 The texture coefficient of **a** CdS, **b** $CdCl_2$-treated CdS films

4.3 Morphological characterization

The SEM images of four different films are presented in Fig. 5a–d. The figure suggests that the cluster sizes have increased with the $CdCl_2$ treatment. Additionally, Fig. 5b shows the established large grains over the course of $CdCl_2$ annealing are made due to the coalescence of small clusters. These coalesced grains could be due to a result of the division of bigger grains into smaller grains and reorienting themselves as discussed earlier, affecting the overall microstructure [36, 37]. As the $CdCl_2$ treatment time increases up to 10 min, spherical clusters about 50–100 nm appear on the surface which have not coalesced together. Pinholes were not found in the film. The increment of the grain size of the $CdCl_2$-treated films can potentially be due to the diffusion of $CdCl_2$ into the CdS film, reorienting the microstructure [16].

4.4 PEC cell characterization

Figure 6 illustrates the variation of V_{OC} and I_{SC} with $CdCl_2$ treatment time. The figure manifests both the superior I_{SC} and V_{OC} values shown by all the films that underwent $CdCl_2$ treatment (Table 3). Consequently, the highest I_{SC} and V_{OC} values were shown by the film S-10. The observed superior I_{SC} values in the $CdCl_2$-coated films potentially resulted from the improved gain size as observed in Fig. 5. Additionally, the highest $I_{SC} \times V_{OC}$ was seen for S-10, suggesting better photoactivity of the film.

Improved electrical properties of $CdCl_2$-treated films can be understood by looking into the structural changes which undergo as a result of the $CdCl_2$ treatment. The presence of Cl^-, resulting from $CdCl_2$ treatment has been identified to act as a fluxing agent that supports the grain growth process [38]. Also, the existence of large grains reduces the number of grain boundaries as well as the scattering of charge carriers at the grain boundaries [38]. Therefore, a detailed explanation of the improvement of electrical properties is worth discussing here.

The mobility of the carriers in the films is affected by several factors including carrier concentration, annealing temperature, and defect complex formation. As the annealing temperature was kept at constant (200 °C) throughout the work, the effect of annealing temperature can be ruled out from the discussion. The increment of the I_{SC} value up to 10 min of $CdCl_2$ treatment time can be attributed from the increment of carrier concentration with the $CdCl_2$ treatment time as shown in Table 3. The decrement in the I_{SC} value beyond the treatment time of 10 min can be due to the increment of charged defect complexes with a growing diffusion concentration of Cl^-. These defect centers surge the scattering rate for the carriers, reducing the mobility of carriers in the deposited films. Additionally, with the increment of Cl diffusion into CdS, vacant centers are filled with charge

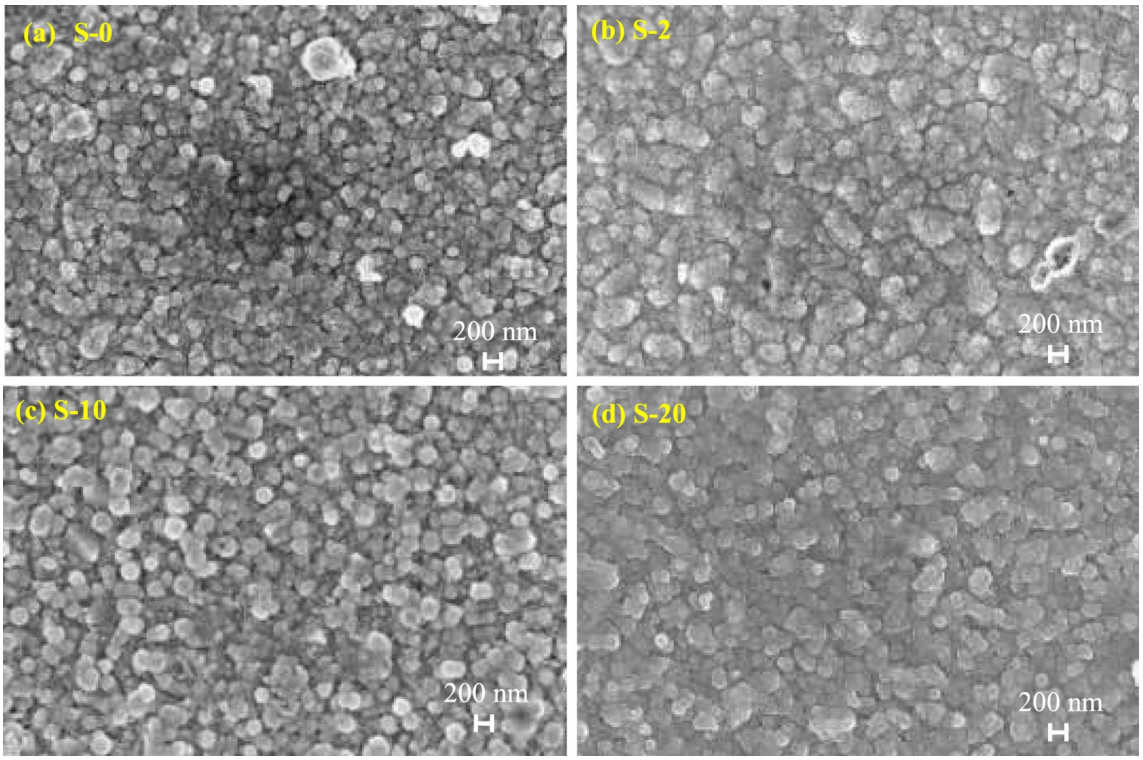

Fig. 5 Scanning electron microscope images of the grown CdS films; **a** $CdCl_2$ treatment time 0 min, **b** $CdCl_2$ treatment time 2 min, **c** $CdCl_2$ treatment time 10 min and **d** $CdCl_2$ treatment time 20 min

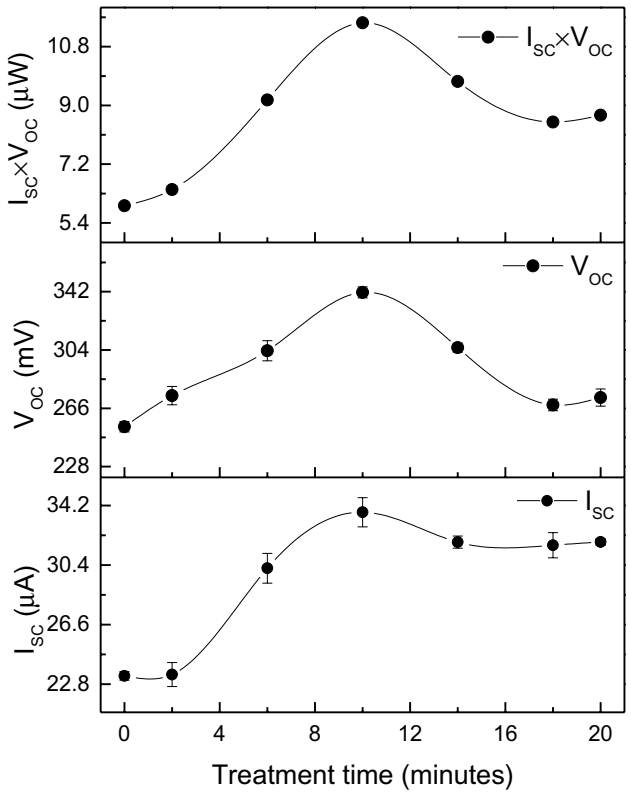

Fig. 6 Open circuit voltage (V_{OC}), short circuit current (I_{SC}) and $I_{SC} \times V_{OC}$ for the $CdCl_2$-treated CdS thin films

carriers. Subsequently, these filled centers create potential barriers near the grain boundary which limits the mobility of carrier charges.

4.5 C–V measurement

Carrier concentration (N_D) and V_{fb} were found from the slope and the X-axis intercept of the linear fit of the Mott-Schottky equation [39]:

$$\frac{1}{C^2} = \frac{2}{A\varepsilon\varepsilon_0 N_D}\left(V - V_{fb} - \frac{kT}{e}\right) \tag{4}$$

where e is the electron charge, A is the area, ε_0 is the permittivity in a vacuum and ε (=8.5) is the dielectric constant [40]. The shape of the gradient of Mott-Schottky plot ($1/C^2$ vs. V) confirms all the grown films are n-type in nature. Fig. 7 and Table 3 show the variation of V_{fb} of grown films corresponding to the $CdCl_2$ treatment time. These results facilitate visualization of the altering nature of the relative energy band edge position in the bandgap of the grown films corresponding to $CdCl_2$ treatment time.

All the $CdCl_2$-treated films showed significantly high V_{fb} (with S-10 presence the highest), suggesting the existence of different energy band edge positions in the $CdCl_2$-treated films compared to untreated. The relative band edge position

Table 3 Variation of electrical and optical bandgap of the $CdCl_2$-treated films

Dipping time (minutes)	I_{SC} (μA)	V_{OC} (mV)	$I_{SC} \times V_{OC}$ (μW)	E_g (eV)	V_{fb} (mV)	N_D (10^{16} cm^{-3})
0	23.32	254.00	5.92	2.33	− 457.77	1.04
2	23.41	274.23	6.42	2.35	− 603.36	1.31
6	30.20	303.5	9.16	2.37	− 611.80	3.84
10	**33.77**	**341.5**	**11.53**	**2.41**	**− 657.05**	**5.11**
14	31.86	305.50	9.73	2.36	− 549.59	4.93
18	31.66	268.16	8.49	2.33	− 562.36	4.85
20	31.87	273.00	8.70	2.34	− 558.75	4.62

Best opto-electrical properties are presented in bold

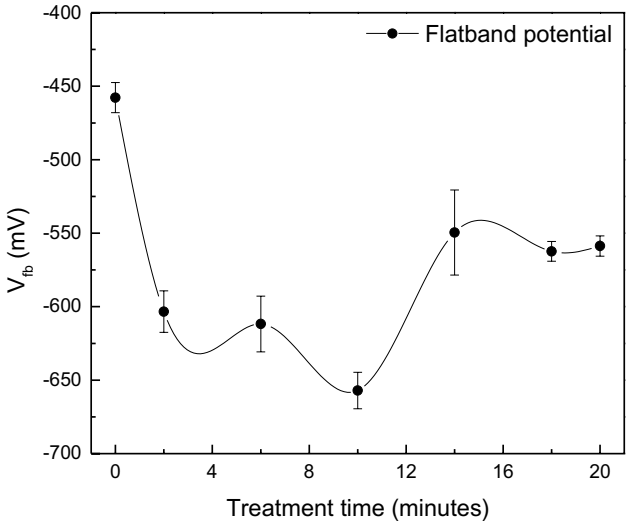

Fig. 7 Flat band potential (V_{fb}) variation of the $CdCl_2$-treated CdS thin films

variation, which is caused by the $CdCl_2$ treatment, can be interpreted in terms of variation of carrier concentration (Table 3) in the material or due to the presence of intermediate energy states. This suggests, as a result of the $CdCl_2$ treatment, the concentration of donor atoms (N_D) increases due to the recrystallization process which in turn improves the ($N_D - N_A$), where N_A is the concentration of acceptors. Additionally, higher V_{fb} produces greater electric field strength in the space charge region, improving the V_{OC} value, hence the photoactivity of the film. Additionally, the tunability of the relative energy band position of the material leads to the improvement of the electrical transport properties of the film, since the formation energy of V_{Cd}^{2+} causes band edge position to shift upwards.

5 Conclusions

$CdCl_2$ treatment has significantly improved the electrical properties of $CdCl_2$-treated films compared to untreated conventional CdS films. The enhancement of V_{OC} in the $CdCl_2$-treated films can be concluded as a result of electrical passivation by $CdCl_2$ and electrons states in the grain boundaries. The superior I_{SC} value seen for $CdCl_2$-treated films can be resulted from the improvement in the grain growth process due to diffusion of Cl^- in to the CdS grains. The E_g value was found to vary from 2.33 to 2.41 eV along with the $CdCl_2$ treatment time with the highest E_g value yielding at a dipping time of 10 min (S-10).

Furthermore, the occurrence of different relative energy band edge positions can also be a reason for the reported better electrical properties of $CdCl_2$-treated CBD-CdS films in comparison to untreated CBD-CdS. Films dipped for 10 min in $CdCl_2$ solution appeared to have the highest flat band potential and V_{OC}.

Therefore, it can be concluded that the tunability of the relative band edge position, higher effective surface area due to higher roughness, recrystallization, and grain boundary passivation due to $CdCl_2$ treatment has enhanced the electrical properties of the grown thin films. Best electrical and optical properties can be achieved with the treatment time of 10 min in $CdCl_2$ solution.

Acknowledgements This work is financially supported by the Solar Edu-Training project of the Ministry of Science, Technology, and Research, Sri Lanka. Part of the research was performed at the Sensor Lab, Department of Information Engineering, Università Degli Studi Di Brescia, Brescia, Italy.

References

1. H. Moualkia, S. Hariech, M.S. Aida, Thin Solid Films **518**, 1259–1262 (2009). https://doi.org/10.1016/j.tsf.2009.04.067
2. L. Wan, Z. Bai, Z. Hou, D. Wang, H. Sun, L. Xiong, Thin Solid Films **518**, 6858–6865 (2010). https://doi.org/10.1016/j.tsf.2010.07.011
3. C.S. Ferekides, D. Marinskiy, V. Viswanathan, B. Tetali, V. Palekis, P. Selvaraj, D.L. Morel, Thin Solid Films **361–362**, 520–526 (2000). https://doi.org/10.1016/S0040-6090(99)00824-X
4. G. Sasikala, R. Dhnasekaran, C. Subramanian, Thin Solid Films **302**, 71–76 (1997). https://doi.org/10.1016/S0040-6090(96)09582-X

5. A. Gupta, V. Parikh, A.D. Compaan, Sol. Energy Mater. Sol. Cells **90**, 2263–2271 (2006). https://doi.org/10.1016/j.solmat.2006.02.029
6. H.C. Chou, A.R. Ohatgi, J. Electron. Mater. **23**, 31 (1994). https://doi.org/10.1007/BF02651264
7. S.A. Al Kuhaimi, Vacuum **51**(3), 349–355 (1998). https://doi.org/10.1016/S0042-207X(98)00112-2
8. O. Savadogo, Chemically and electrochemically deposited thin films for solar energy materials. Sol. Energy Mater. Sol. Cells **52**, 361–368 (1998). https://doi.org/10.1016/S0927-0248(97)00247-X
9. E.X. Mathew, Sol. Energy Mater. Sol. Cells **76**, 313–325 (2003). https://doi.org/10.1016/S0927-0248(01)00090-3
10. W.G.C. Kumarage, R.P. Wijesundera, V.A. Seneviratne, C.P. Jayalath, B.S. Dassanayake, J. Phys. D. Appl. Phys. **49**, 95109 (2016). https://doi.org/10.1088/0022-3727/49/9/095109
11. W.G.C. Kumarage, L.B.D.R.P. Wijesundara, V.A. Seneviratne, C.P. Jayalath, B.S. Dassanayake, Procedia Eng. **139**, 64–68 (2016). https://doi.org/10.1016/j.proeng.2015.09.215
12. W.G.C. Kumarage, R.P. Wijesundera, V.A. Seneviratne, C.P. Jayalath, T. Varga, M.I. Nandasiri, B.S. Dassanayake, Mater. Chem. Phys. **200**, 1–8 (2017). https://doi.org/10.1016/j.matchemphys.2017.07.052
13. W.G.C. Kumarage, L.B.D.R.P. Wijesundara, V.A. Seneviratne, C.P. Jayalath, B.S. Dassanayake, Semicond. Sci. Technol. **32**, 045014 (2017). https://doi.org/10.1088/1361-6641/aa5ee3
14. F. Liu, Y. Lai, J. Liu, B. Wang, S. Kuang, Z. Zhang, J. Li, Y. Liu, J. Alloy. Compd. **493**, 305–308 (2010). https://doi.org/10.1016/j.jallcom.2009.12.088
15. M. Tsuji, T. Aramoto, H. Ohyama, T. Hibino, K. Omura, Jpn. J. Appl. Phys. **39**, 3902–3906 (2000). https://doi.org/10.1143/JJAP.39.3902
16. I.M. Dharmadasa, Coatings **4**, 282–307 (2014). https://doi.org/10.3390/coatings4020282
17. J. Salinger, J. Acta Polytechnica **46**, 25–27 (2006)
18. M.J. Kim, J.J. Lee, S.H. Lee, S.H. Sohn, Solar Energy Mater. Solar Cells **109**, 209–214 (2013). https://doi.org/10.1016/j.solmat.2012.11.012
19. D.B. Laks, C.G. Van de Walle, G.F. Neumark, S.T. Pantelides, Phys. Rev. Lett. **66**, 648–651 (1991)
20. M.A. Islam, M.S. Hossain, M.M. Aliyu, M.R. Karim, T. Razykov, K. Sopian, N. Amin, Thin Solid Films **546**, 367–374 (2013). https://doi.org/10.1016/j.tsf.2013.04.067
21. J. Lee, Curr. Appl. Phys. **11**(1), 103–108 (2011). https://doi.org/10.1016/j.cap.2010.11.099
22. A. Rios-Flores, J.L. Peña, V. Castro-Peña, O. Ares, R. Castro-Rodríguez, A. Bosio, Sol. Energy **84**(6), 1020–1026 (2010). https://doi.org/10.1016/j.solener.2010.03.010
23. W.G.C. Kumarage, R.P. Wijesundera, V.A. Seneviratne, C.P. Jayalath, T. Varga, B.S. Dassanayake, Appl. Phys. A **124**, 494 (2018). https://doi.org/10.1007/s00339-018-1910-0
24. K.K.M.B.B. Adikaram, W.G.C. Kumarage, T. Varga, B.S. Dassanayake, J. Electron. Mater. **48**(7), 4424–4431 (2019). https://doi.org/10.1007/s11664-019-07215-5
25. W.G.C. Kumarage, R.P. Wijesundera, V.A. Seneviratne, C.P. Jayalath, N. Kaur, E. Comini, B.S. Dassanayake, J. Photochem. Photobiol. A **367**, 171–177 (2018). https://doi.org/10.1016/j.jphotochem.2018.08.029
26. A. Oliva-Avilés, R. Patiño, A. Oliva, Appl. Surf. Sci. **256**, 6090–6095 (2010). https://doi.org/10.1016/j.apsusc.2010.03.125
27. A. Mukherjee, P. Ghosh, A.A. Aboud, P. Mitra, Mater. Chem. Phys. **184**, 101–109 (2016). https://doi.org/10.1016/j.matchemphys.2016.09.030
28. A.I. Oliva, O.S. Canto, R.C. Rodrigues, P. Quintana, Thin Solid Films **391**(1), 28–35 (2001). https://doi.org/10.1016/S0040-6090(01)00830-6
29. A. Kariper, E. Güneri, F. Gödethe, C. Gümüs, T. Özpozan, Mater. Chem. Phys. **129**, 183–188 (2011). https://doi.org/10.1016/j.matchemphys.2011.03.070
30. S.A. Ringel, A.W. Smith, M.H. MacDougal, A. Rohatgi, J. Appl. Phys. **70**(2), 881 (1991). https://doi.org/10.1063/1.349652
31. A. Luque, S. Hegedus, *Handbook of photovoltaic science and engineering* (John Wiley & Sons, Chichester, 2011)
32. S. Du, Y. Li, Adv. Mater. Sci. Eng. **2015**, 8 (2015). https://doi.org/10.1155/2015/969580
33. V. Bilgin, S. Kose, F. Atay, I. Akyuz, J. Mater. Sci. **40**, 1909–1915 (2005). https://doi.org/10.1007/s10853-005-1210-x
34. P.K.K. Kumarasinghe, A. Dissanayake, B.M.K. Pemasiri, B.S. Dassanayake, Mat. Sci. Semicon. Proc. **58**, 51–60 (2017). https://doi.org/10.1016/j.mssp.2016.11.028
35. P.K.K. Kumarasinghe, A. Dissanayake, B.M.K. Pemasiri, B.S. Dassanayake, Mater. Res. Bull. **96**, 188–195 (2017). https://doi.org/10.1016/j.materresbull.2017.04.026
36. H.R. Moutinho, R.G. Dhere, M.M. Al-Jassim, D.H. Levi, L.L. Kazmerski, J. Vac. Sci. Technol. **A17**, 1793 (1999). https://doi.org/10.1116/1.581892
37. A. Nawaz, Z. Rabeel, N.A. Shah, World Appl. Sci. J. **31**(8), 1522–1530 (2014). https://doi.org/10.5829/idosi.wasj.2014.31.08.621
38. P.K.K. Kumarasinghe, A. Dissanayake, B.M.K. Pemasiri, B.S. Dassanayake, J. Mater. Sci.: Mater. Electron. **28**, 276–283 (2017). https://doi.org/10.1007/s10854-016-5521-2
39. M. Akif, S. Aliyev, M. El-Rouby, Int. J. Thin Film Sci. Technol. **2**, 195–2005 (2013). https://doi.org/10.12785/ijtfst/020305
40. W.G.C. Kumarage, R.P. Wijesundera, N. Kaur, D. Zappa, V.A. Seneviratne, C.P. Jayalath, B.S. Dassanayake, Int. J. Electroact. Mater. **7**, 1–6 (2019)